

Charge exchange and energy loss of particles interacting with surfaces

A. Nürmann and W. Heiland

Universität Osnabrück, Fachbereich Physik, Barbarastrasse 7, D-4500 Osnabrück, Federal Republic of Germany

R. Monreal and F. Flores

Universidad Autónoma de Madrid, Departamento de la Materia Condensada, C XII, Cantoblanco, E-28049 Madrid, Spain

P. M. Echenique

Euskal Herriko Unibertsitatea, Kimika Fakultatea, Fisika Saila, Apartado 1072, E-20080 San Sebastián, Spain

(Received 31 October 1990; revised manuscript received 9 April 1991)

The charge state and energy loss of low-energy He ions scattered off a Ni(110) surface have been measured using a time-of-flight technique. A first-principles theory in combination with trajectory calculations is used to analyze both the charge-state and the energy-loss data. The neutralization of the incident He ions occurs via the Auger process. We find that the experimental results for the energy loss can only be explained when accounting for the charge exchange during the interaction and for straggling effects. The change of the charge state appears in the spectra through the asymmetry, whereas the straggling shows up as a broadening of the peak.

I. INTRODUCTION

Two of the most important physical properties accompanying the interaction of particles with metal surfaces are the charge state of the particles and the energy lost in the course of scattering. Since charge state and energy loss are interrelated, they can hardly be understood on their own.

The scattered particles include surviving ions, neutralized ones, and reionized particles—possibly more than once—as well as such particles changing the sign of their charge during the interaction (e.g., $H^+ \rightarrow H^0 \rightarrow H^-$). For a given target the yield of the different charge states depends strongly on the energy of the incident particles, the angle of incidence and on the crystallographic direction along which they are scattered.

The energy loss of particles scattered into a certain charge state depends on the history of the particle during the interaction with the surface (i.e., multiple reionization and neutralization) as well as on the incident energy, incident angle, and azimuthal direction. The first report—to our knowledge—on the influence of charge changing collisions on the energy loss was by Allison in the late fifties.¹

The aim of this work is to shed some light on this interrelationship between energy loss and charge exchange and to point out how the physical effects influence each other.

This work is a continuation and an extension of our recently published results;² for a more extensive review on earlier work see Ref. 3. The paper is divided into three parts: First, the experiments will be described, i.e., the experimental setup used, the results obtained as well as the computational calculations performed with the MAR-

LOWE code. (Since MARLOWE simulates an experiment, it belongs to this section.) In the second part the theory used to explain the experimental findings will be presented, and finally a comprehensive discussion will be given.

II. EXPERIMENTS

The experiments were performed in an ultra-high-vacuum (UHV) system with a base pressure of about 2.0×10^{-10} mbar described in detail in Ref. 4. The heart of the apparatus is a time-of-flight (TOF) system with the TOF tube placed at a scattering angle of 10° . In an acceleration stage the charged particles leaving the surface can be separated from the neutrals. The detector has an angle of acceptance of 1.2° (full width). In the energy region used in the experiments the detector efficiency is the same for ions and neutral particles.⁵ The time resolution at 1 keV is 5 ns. The target is mounted onto a manipulator, which allows for variation of the azimuthal and incident angle. In the experiments to be described the incident angle was fixed at 5° .

From the scattered beam the charge states and the energy loss were detected. For the experiments a clean Ni(110) surface was used. The cleanliness of the surface was checked by ion-scattering spectrometry (ISS) using an electrostatic energy analyzer at a scattering angle of 90° as well as by monitoring the width of the TOF distribution of the scattered particles. The preparation of the crystal was achieved *in situ* by prolonged sputtering with 1–2 keV Ne^+ ions at small incident angle (less than 3°) with simultaneously varying the azimuthal angle and subsequent annealing. This procedure was repeated until (a) in the IS spectrum only non-Ni peaks with an intensity of less than 1% of the Ni peak appeared (which was

achieved 1 or 2 days after the crystal was brought into UHV) and (b) the width of the TOF distribution of the scattered particles did not decrease any more (which took up to 2 weeks). In this way we have minimized contributions to the width of the peak by steps and defects on the surface. Once the width was minimized, a clean surface—in the sense described above—could be obtained by a few hours of small-angle sputtering and subsequent annealing. The quality of the surface structure after this treatment was checked by low-energy electron diffraction (LEED). From former LEED measurements on a different Ni(110) crystal a terrace length of about 100 Å was deduced.⁶

Surface imperfections tend to enhance the background and broaden the angular (azimuth) as well as the energy distribution of the detected particles. The calibration of the primary beam energy, the beam spread on the target and the scatter of the TOF data add up to errors of about ± 10 eV in the 1–5 keV incident energy range.

A. Measurements of charge state

After scattering a He^+ beam with an energy of 2–5 keV off a Ni(110) surface, the ions were accelerated in the TOF tube to clearly separate the ions from the neutral particles in the TOF spectra. For an incident energy less than 2 keV the ion yield is too small to be measured with good enough accuracy; above 5 keV the post-acceleration voltage becomes insufficient to distinctly separate the ion and the neutral peak. A typical TOF spectrum is shown in Fig. 1. The peak at shorter time corresponds to faster particles in the scattered beam, i.e., in this case ions.

For each azimuthal angle the neutral and the ion peaks have been integrated. The ion yield obtained in this way includes both surviving and reionized ions. As we will show later, surviving and reionized ions suffer different energy losses, and hence it should be possible to see two

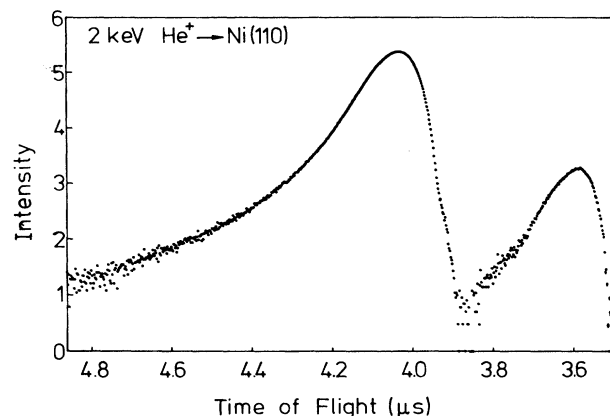


FIG. 1. Time-of-flight spectrum of He^+ incident on Ni(110). The peak on the right (shorter time) corresponds to reionized particles and the one on the left to neutral particles. The intensity scale is logarithmic. Separation of the peaks was achieved by applying a post-acceleration voltage of 1500 V. Note that the time axis runs from the right to the left.

peaks corresponding to ions in the TOF spectra. But unfortunately the distance between the post-acceleration stage and the detector is too short in our TOF system to resolve those two peaks. A simple calculation (assuming a ratio of 3.7 for the friction coefficient of an ion to the friction coefficient of a neutral particle, see Sec. IV) shows that, e.g., in Fig. 1 the peak corresponding to surviving ions should appear at $3.7 \mu\text{s}$, i.e., still in the tail of the peak of the reionized particles.

The azimuthal angles have been chosen to include the two major crystallographic directions: $[\bar{1}10]$ at $\phi=0^\circ$ and $[001]$ at $\phi=90^\circ$. Figure 2 shows the angular dependence of the neutral yield for different energies. The ion yield is given in Fig. 3, and the azimuthal dependence of the charged fraction, defined as

$$\frac{Y(\text{He}^+)}{Y(\text{He}^+) + Y(\text{He}^0)},$$

where $Y(x)$ stands for yield of x , is plotted in Fig. 4. The results are similar for all energies: (a) maxima of the ion and neutral yield in $[\bar{1}10]$ and $[001]$ directions and (b) minima of the charge state fraction in the crystallographic directions although the ion yield exhibits maxima in

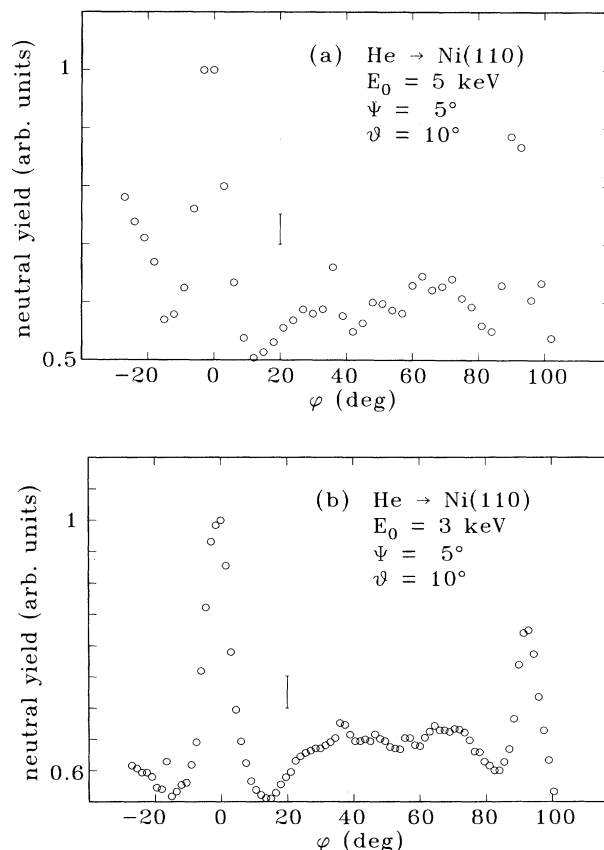


FIG. 2. Azimuthal dependence of the yield of neutralized He ions when scattered off a Ni(110) surface. Incident angle was 5° , and scattering angle was 10° .

these directions; i.e., in the surface channel directions there are actually less ions than for random directions. ("Random" signifies a no-low-index direction.)

B. Measurements of energy loss

To determine the energy lost in the course of scattering, the TOF spectra were converted into energy spectra. Then, after evaluating the primary energy by deflecting the primary beam into the TOF tube, the energy loss could easily be calculated. Figure 5 shows the energy spectra of reflected neutrals scattered along random direction for different incident energies. The peaks are asymmetric: The low-energy tail falls off more slowly than the high-energy tail, in contrast to the spectra calculated for somewhat higher incident energies in Ref. 7, where the shapes are well described by Gaussians. The asymmetry is even more obvious in the spectra obtained after scattering along crystallographic directions. Figure 6 shows the energy distribution of neutrals after 3-keV He^+ scattering off Ni(110) along $[\bar{1}10]$ and $[001]$. Figure 7 shows the energy distribution of He^+ scattered along a random direction off Ni(110) (and leaving the surface as ions).

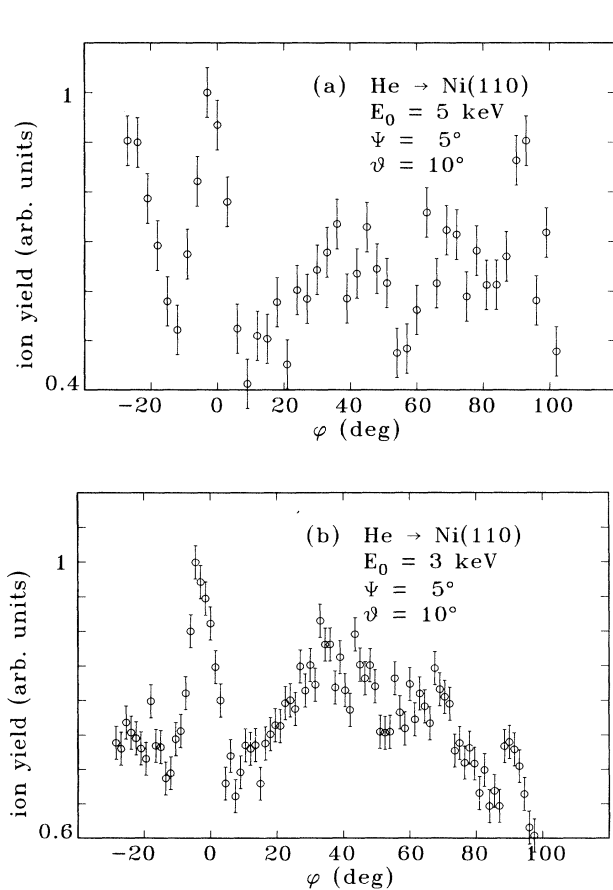


FIG. 3. Azimuthal dependence of the yield of He ions when scattered off a Ni(110) surface. Incident angle was 5° , and scattering angle was 10° .

Because in the case of the ion spectra we cannot separate the surviving ions from the reionized particles (see Sec. II A), we will not discuss the spectra of outgoing ions in more detail. The surviving ions appear in the tail of the ion spectrum and, hence, do contribute in the same way as reionized particles with a larger energy loss.

C. Calculations of the particle trajectories

Figures 2 and 3 show that there are maxima of the ion and the neutral yield in the crystallographic directions, due to surface channeling.⁸ The strong steering becomes evident by inspection of the data of the MARLOWE simulations.^{9,10}

MARLOWE describes the collisions of the incoming particle with target atoms in a binary-collision approximation. Between the collisions the particles move along straight lines, the asymptotes of their paths in the laboratory system. Thermal vibrations were taken into account by randomly choosing the atomic lattice positions according to a surface Debye temperature of 200 K.¹¹ The inclusion of the Debye temperature is important; omitting it leads to features that are much too sharp compared to the experiments. Image charge effects are not

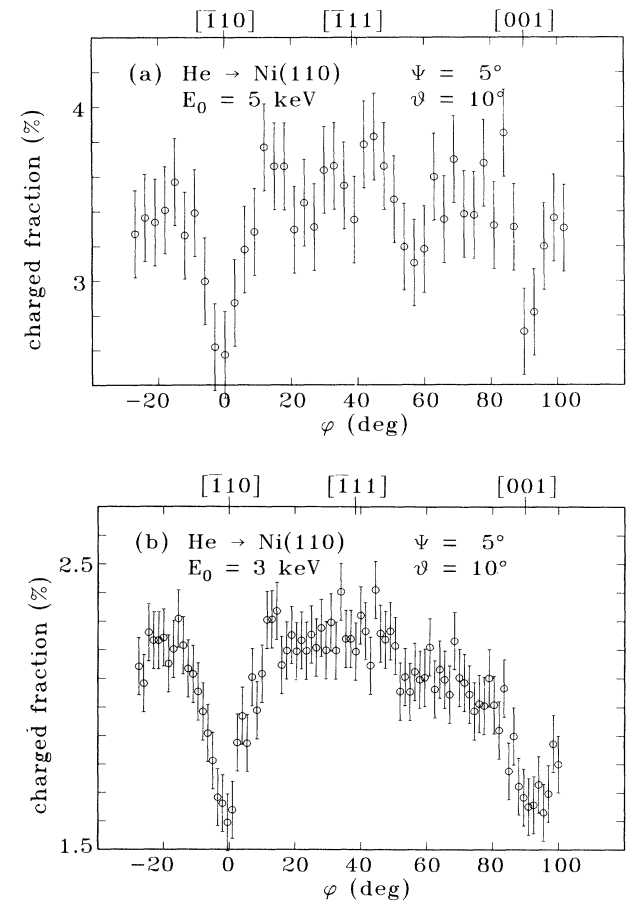


FIG. 4. Charge-state fraction as defined in the text as a function of azimuthal angle for different energies.

accounted for, but in our case this is a reasonable assumption, since the Auger neutralization to the ground state is very fast (see Sec. III A) and we are dealing with particles that are neutral practically along the whole trajectory. The results shown below are based on 20 000 incident He particles. The potential used is the Ziegler-

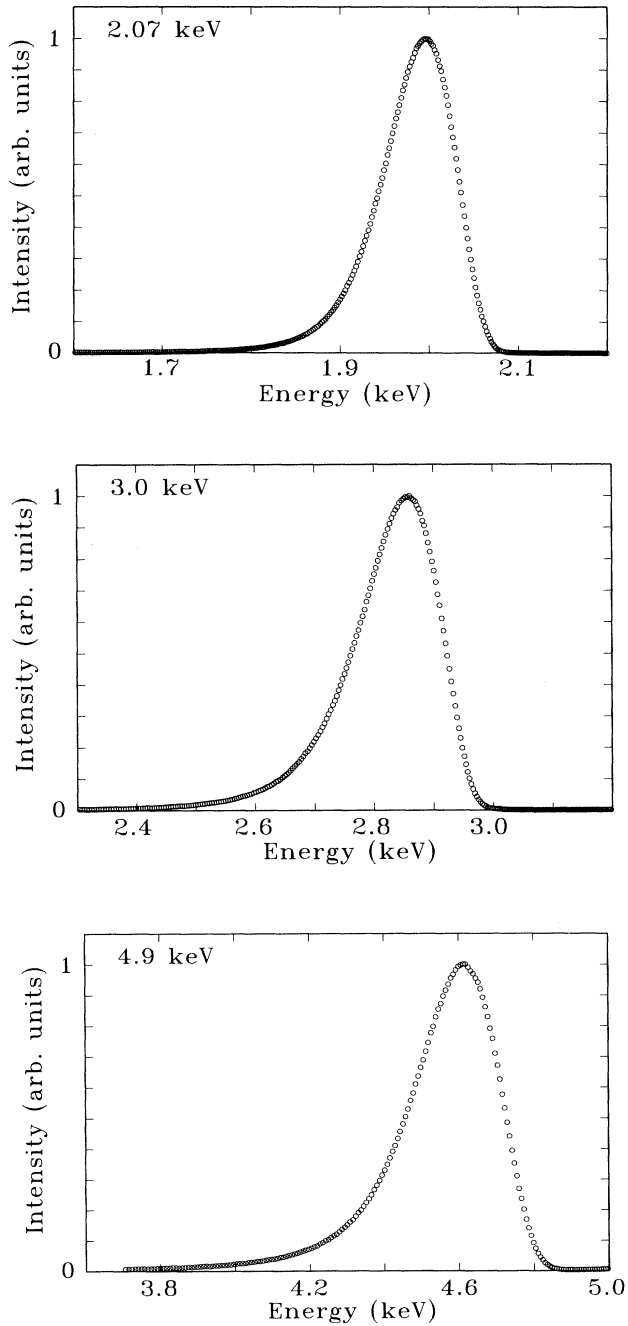


FIG. 5. Energy spectra of reflected neutral particles for different incident energies in random direction. Incident angle of incoming He ions was 5° , and scattering angle was 10° .

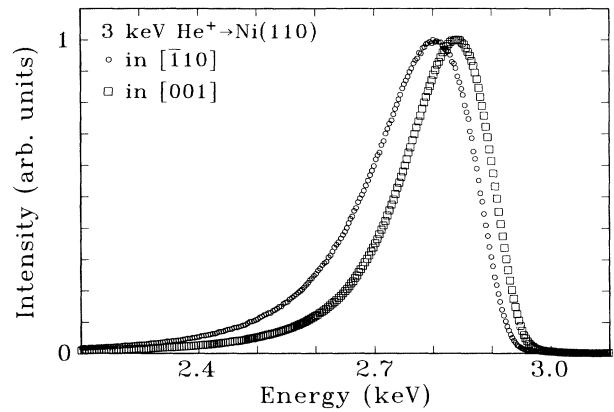


FIG. 6. Energy spectra of reflected neutral particles for a 3-keV incident energy in crystallographic directions. Incident angle of incoming He ions was 5° , and scattering angle was 10° .

Biersack-Littmark (ZBL) potential,¹² which gives better agreement with the experiment than the Thomas-Fermi-Molière (TFM) potential.¹³

Figure 8 shows the azimuthal dependence of the penetration depth of the detected particles only as well as of all reflected particles. The results for the reflection coefficient are shown in Fig. 9. The minima are related to the structure of the crystal surface, i.e., in channel direction some particles penetrate into the bulk and escape detection.

Two sets of trajectories in the side and the top view are plotted in Fig. 10 for two different azimuthal directions. The trajectories shown are a randomly chosen subset out of the 20 000 incident particles. As already shown by the penetration depth data the trajectories in the random

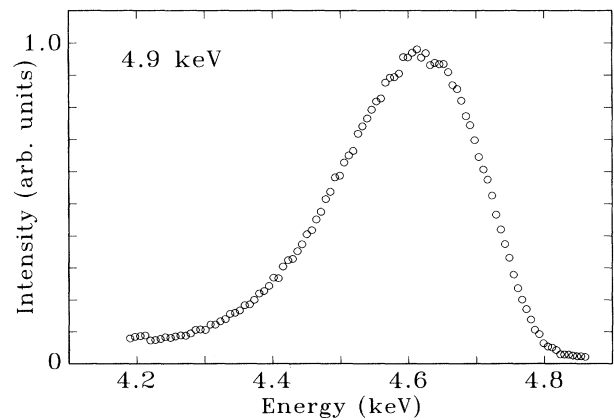


FIG. 7. Energy distribution of He^+ scattered along a random direction off Ni(110). The energy scale shown is not exact due to uncertainties in the determination of the post-acceleration voltage.

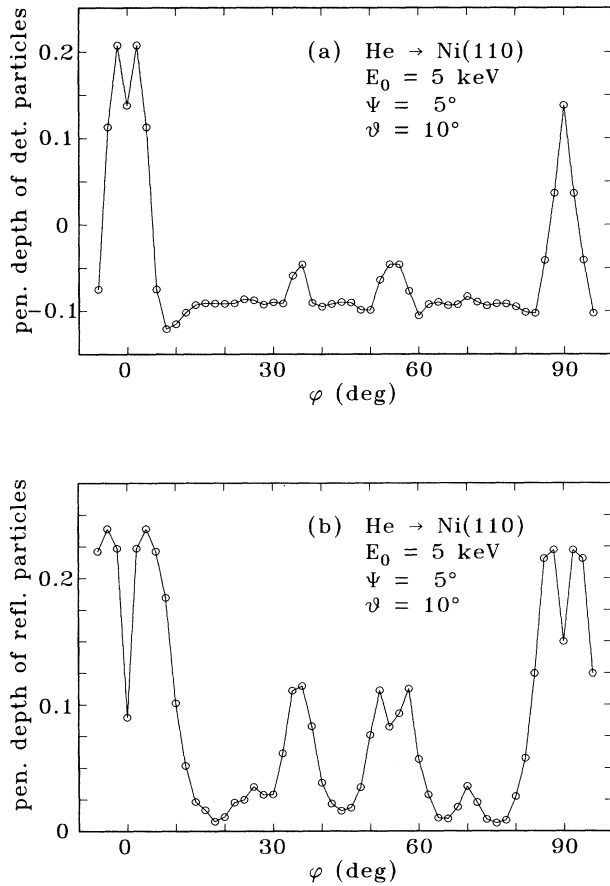


FIG. 8. Penetration depth of all detected (top) and all reflected (bottom) particles in units of the lattice constant $d_0 = 3.51 \text{ \AA}$.

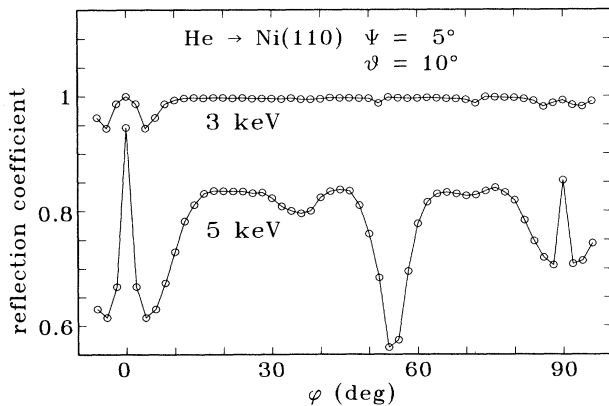


FIG. 9. Azimuthal dependence of the particle reflection coefficient for 3- and 5-keV incident energy.

direction do not penetrate the outermost layer, whereas in the channel direction the particles are steered between the surface rows. For a more detailed analysis of the MARLOWE data see Ref. 14.

III. THEORY

There exists a large amount of literature concerning charge exchange and energy loss processes. Theoretical investigations on the charge state of particles scattered from surfaces are given, e.g., in Refs. 15–23; treatments on the energy loss of particles scattered from surfaces include Refs. 24–28.

In the following we will describe charge exchange and energy loss of a He particle at a Ni(110) surface in terms of *bulk* properties expressed by the bulk dielectric response function, which of course requires justification. Following the arguments given by Lang,²⁹ the “effective” surface is positioned at a distance D above the last atomic layer with $D = x_0 + \frac{1}{2}d$, where d is the interplanar spacing (for Ni: $d = 2.55 \text{ a.u.}$) and x_0 is the center of mass of the induced charge-density distribution (for $r_s = 2$ is $x_0 = 1.6 \text{ a.u.}$). Since for Ni $r_s < 2$, we get $D = 1.52 \text{ \AA}$ as a lower limit for the distance of the effective surface in front of the outermost lattice plane.

This is to be compared on the one hand with the results of the MARLOWE calculations (see Sec. II C) according to which the He particles (in the energy range investigated here) approach the last atomic layer to a distance of 0.4 \AA —i.e., clearly *below* the effective surface—and on the other with the decay length for the Auger-transition rate, which is 1.3 \AA (see Sec. III A).

We also calculated the Auger-neutralization rate using the surface dielectric function (using roughly the same model as outlined below), but the results do not agree with the experimental numbers (thus giving further indirect support for our approach).

A. Charge exchange processes

Two mechanisms seem to be most important in He^+ neutralization: the Auger capture and resonant tunneling from a metal state to the empty $2s$ state with subsequent Auger deexcitation to the ground state. The second process is only effective if the energy of the $2s$ level lies below the Fermi energy. But for He^+ the metastable $2s$ level crosses the Fermi energy at such a large distance away from the surface that no electronic transition can occur here.¹⁵ In the following we will use atomic units throughout.

1. Interaction of an ion with an electron gas

The Hamiltonian of the system, H , consists of the Hamiltonian of the electron gas H_0 , the Hamiltonian for the ion H_I , and an interaction term V :

$$H = H_0 + H_I + V,$$

where H_I and V are given by

$$H_I = -\frac{1}{2M} \nabla_{\mathbf{R}_I}^2 + H_{\text{internal}},$$

$$V = \sum_j \frac{Z_I}{|\mathbf{r}_j - \mathbf{R}_I|} = \int d\mathbf{r} \frac{Z_I \rho(\mathbf{r})}{|\mathbf{r} - \mathbf{R}_I|}.$$

The vector \mathbf{r}_j points to the j th electron in the electron gas, \mathbf{R}_I points to the ion center of mass, and H_{internal} refers to the internal structure of the ion. Z_I is the charge of the ion, and M is its mass. $\rho(\mathbf{r})$ is the particle-density operator given by

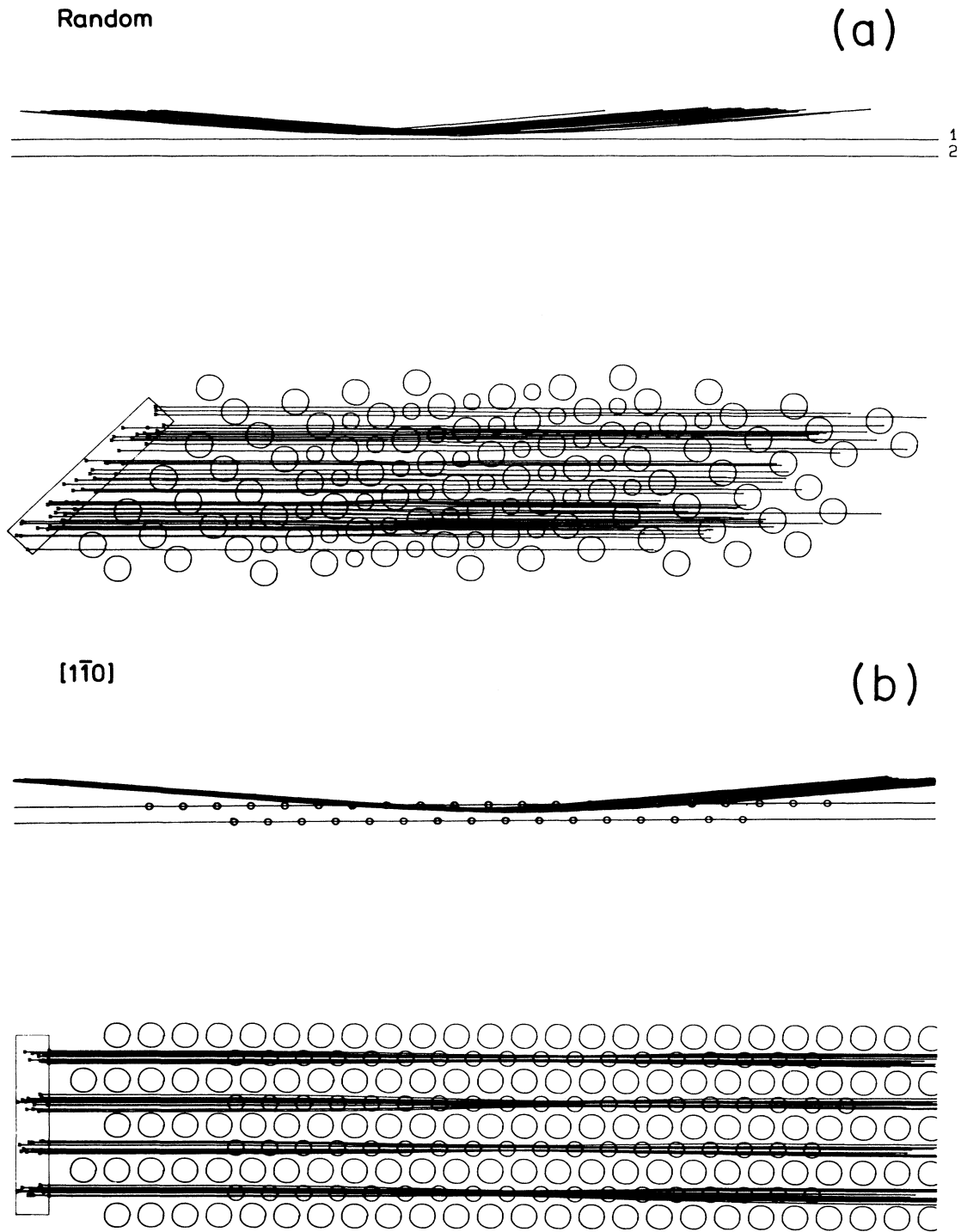


FIG. 10. Particle trajectories for 3-keV He scattered off Ni(110) in two different azimuthal directions.

$$\rho(\mathbf{r}) = \sum_j \delta(\mathbf{r} - \mathbf{r}_j) .$$

The initial state is given by

$$|i\rangle = e^{i\mathbf{k}\cdot\mathbf{R}_I} |\phi_{\text{internal}}\rangle e^{i\mathbf{k}_i\cdot\mathbf{r}'} ,$$

which fulfills

$$H_I |i\rangle = E_i |i\rangle, \quad E_i = \frac{k^2}{2M} + \frac{1}{2} k_i^2 + E_{\text{internal}}$$

with \mathbf{k} being the momentum of the ion, \mathbf{k}_i the momentum of the electron, and E_i the energy in the initial state. $|\phi_{\text{internal}}\rangle$ and E_{internal} are the wave function and energy, respectively, of the ion and $e^{i\mathbf{k}_i\cdot\mathbf{r}'}$ represents the free electron jumping into the He 1s state. After capturing an electron, the final state is

$$|f\rangle = e^{i\mathbf{k}_0\cdot\mathbf{R}} |\phi_{\text{internal}}\rangle u_0(\mathbf{r}')$$

$$\frac{1}{\tau_A} = \int_{-\infty}^{\infty} \frac{d^3q}{(2\pi)^3} \int_0^{\infty} \frac{d\omega}{2\pi} \sum_{\mathbf{k}_i} \Theta(k_F - |\mathbf{k}_i + \mathbf{v}|) \frac{16\pi^2}{q^2} \delta\left(\omega - \frac{k_i^2}{2} - \mathbf{q}\cdot\mathbf{v} + \omega_0\right) \mathcal{J} \left[\frac{-1}{\epsilon(\mathbf{q}, \omega)} \right] |\langle u_0(\mathbf{r}') | e^{-i\mathbf{q}\cdot\mathbf{r}'} | e^{i\mathbf{k}_i\cdot\mathbf{r}'} \rangle|^2 ,$$

where ω and \mathbf{q} are the energy and momentum of the excitation in the solid, \mathbf{k}_F is the Fermi wavevector, and \mathbf{v} is the velocity of the ion core; v has been taken to be constant before and after the collision. In our case, however, for the low incident energy regime, v is small enough to be taken as $v \simeq 0$ with a good accuracy.

\mathcal{J} denotes the imaginary part, and $\epsilon(\mathbf{q}, \omega)$ is the dielectric function of bulk nickel, which has been approximated by a local one, $\epsilon_{\text{Ni}}(\omega)$, with an appropriate cutoff in q :

$$\epsilon(\mathbf{q}, \omega) = \epsilon_{\text{Ni}}(\omega) \Theta(q_c - q) ,$$

where $\epsilon_{\text{Ni}}(\omega)$ was taken from the data compiled in Ref. 31 and q_c was introduced to describe the decay of the dielectric function for large q ; q_c is expected to lie between the Fermi wavelength $q_F \simeq 0.7$ a.u.—corresponding to s electrons—and $q_d \simeq 2.0$ a.u. associated

$$\frac{1}{\tau_A} = \sum_{\mathbf{R}_j} \int_{-\infty}^{\infty} \frac{d^3q}{(2\pi)^3} \int_0^{\infty} \frac{d\omega}{2\pi} \frac{16\pi^2}{q^2} \sum_{\alpha} \int_0^{E_F} \rho_{\alpha}(E) dE \delta(\omega + E - \omega_0) \mathcal{J} \left[\frac{-1}{\epsilon(\mathbf{q}, \omega)} \right] |\langle u_0(\mathbf{r}') | e^{-i\mathbf{q}\cdot\mathbf{r}'} | \alpha \rangle|^2 ,$$

where $\rho_{\alpha}(E)$ is the density of states associated with the orbital Φ_{α} .

For computation the Ni-4s, Ni-3d, and He-1s wave functions have been taken from Ref. 32 and the density of

TABLE I. Maximum transition probabilities for different cutoffs and the decay lengths corresponding to s and d electrons.

	$q_c = 1$ a.u.	$q_c = 1.5$ a.u.	
$\tau_{A,s}$	2.8×10^{-15} s	1.1×10^{-15} s	$1.3 \text{ \AA} = d_s$
$\tau_{A,d}$	1.7×10^{-15} s	4.8×10^{-16} s	$0.4 \text{ \AA} = d_d$

with energy

$$E_f = \frac{k_0^2}{2(M+1)} + \omega_0 + E_{\text{internal}} .$$

There \mathbf{k}_0 is the total momentum of the ion-electron composite,

$$\mathbf{R} = \frac{1}{M+1} (\mathbf{r}_e + M\mathbf{R}_I)$$

is the center of mass, \mathbf{r}_e is the coordinate vector of the electron in the composite, u_0 is the wave function (with energy ω_0) describing the relative motion of the electron in the composite with respect to the ion, and $\mathbf{r}' = \mathbf{r}_e - \mathbf{R}_I$.

The Fermi golden rule then gives the transition probability per unit time for the transition $|i\rangle|0\rangle \rightarrow |f\rangle|n\rangle$, where $|n\rangle$ denotes an eigenvector of the homogeneous electron gas. For details of the calculation see, e.g., Ref. 30. The resulting Auger-transition rate is

with the momentum of the d electrons.

The metal wave function was orthogonalized to the atomic one by means of

$$|\mathbf{k}_i\rangle = \Psi_{\mathbf{k}_i} - \langle u_0 | \Psi_{\mathbf{k}_i} \rangle u_0(\mathbf{r}) ,$$

where $\Psi_{\mathbf{k}_i}$ is the crystal Bloch function, which has been written as a linear combination of atomic functions: $\Psi_{\mathbf{k}_i} = \sum_{\mathbf{R}_j} e^{-i\mathbf{k}_i\cdot\mathbf{R}_j} |\alpha\rangle$, where

$$|\alpha\rangle = |\Phi_{\alpha}\rangle - \langle u_0 | \Phi_{\alpha} \rangle |u_0\rangle ,$$

and $\Phi_{\alpha}(\mathbf{r} - \mathbf{R}_j)$ are the localized wave functions for the orbital α of the atom at site \mathbf{R}_j .

As a further approximation the interference terms between the different sites were neglected, i.e., instead of $\Psi_{\mathbf{k}_i}$ now $\Phi_{\alpha}(\mathbf{r}) - \langle u_0 | \Phi_{\alpha} \rangle |u_0\rangle$ was used. This leads to

states for s and d electrons we took from Ref. 33. The resulting transition rates, as well as the corresponding $1/e$ decay lengths, are listed in Table I for two different cutoffs. From there we conclude, that the effect of the d electrons is negligible because of the much shorter decay length.

2. Other mechanisms of charge exchange

Here we give a very short summary of other charge exchange processes and discuss the relevance for our case.

a. Inner shell processes. For high velocities, close

atom-atom collisions are dominant³⁴ and capture of inner-shell electrons is possible. The cross sections associated with this process have been analyzed in Ref. 35 for high ($v \gg 1$) and intermediate ($v \simeq 1$) velocities. In the velocity range used in this work inner-shell capture is of no importance.

b. Dynamic resonant processes. These are induced by the periodic lattice potential, which the ion sees as a time-dependent perturbation when traveling along the surface.³⁵ The probability per unit time of having a dynamic resonant loss is given by

$$\frac{1}{\tau_R} = 2\pi \sum_{|\mathbf{k}+\mathbf{v}| > k_F} \sum_{\mathbf{g}} |V_{\mathbf{g}}|^2 |\langle s | e^{+i\mathbf{g}\cdot\mathbf{r}} | \mathbf{k} \rangle|^2 \times \delta(E_0 - \frac{1}{2}k^2 + \mathbf{g}\cdot\mathbf{v})$$

with \mathbf{g} being a reciprocal lattice vector and $V_{\mathbf{g}}$ the Fourier transform of the crystal potential. This loss process will be used in the discussion to explain azimuthal effects.

A similar formula holds for capture and is obtained by replacing the $>$ sign under the sum by a $<$ sign and substituting the plus signs in the exponential and in the argument of the δ term by minus signs. In the derivation of these formulas interference effects between different reciprocal lattice vectors (those satisfying $\mathbf{g}\cdot\mathbf{v} = \mathbf{g}'\cdot\mathbf{v}$ have been neglected; i.e., effects associated with channeling are not included.

The cross sections for the different capture and loss processes are shown, e.g., in Figs. 21 and 23 of Ref. 30. From there we conclude that for capture processes the Auger process overwhelms all other mechanisms in our velocity range and that the only loss process active is dynamic resonant loss.

B. Energy loss and straggling

In low-energy ion scattering there are two different types of energy losses. The discrete losses^{36–38} are mostly understood in terms of electron promotion models based on a theory developed in Ref. 39. In our case the impact parameter is too large for those processes to be active.

The other kinds of losses are observed as a shift of the elastic peak position as well as a broadening of the energy loss spectrum on the low-energy side.^{40,41} These peak shapes are difficult to understand, since in most experiments they are affected by neutralization, and—depending on the geometry used—multiple scattering may contribute, too.

In the literature there are two different approaches dealing with energy losses associated to the motion of a charge or an atom near a metal surface. The energy dissipated to a metal surface was calculated by a friction coefficient method^{42,26} and by a dynamical approach based on the dielectric surface response.^{43–45}

The friction coefficient method is based on a Brownian motion formalism to treat the kinetics of chemicals near metal surfaces. Sols, Miranzo, and Flores²⁴ have shown that in the low-velocity limit the dynamical approach yields the same results as the friction coefficient method.

This implies that the friction coefficient can be expressed in terms of the bulk dielectric function.

In the following we will concentrate on the energy loss experienced by the particles in the interaction region (we shall estimate later the loss suffered before and after penetration into this region) and write for the differential energy loss $dQ_+ = \gamma_s^+ v ds$ for ions and $dQ_0 = \gamma_s^0 v ds$ for neutral particles, where γ_s^+ and γ_s^0 are the surface friction coefficients.

Up to now we only considered differential energy losses $dQ^{0,+}$ from which the total energy loss is obtained by integrating this quantity over the distance the particle interacts with the surface. We did not account for effects arising from the energy distribution in a *single* collision. (In our case these are electron-hole-pair excitations.) This will affect the energy loss, since it is the cumulative result of a large number of collisions and because this energy distribution is different for ions and neutrals.

Those effects will lead to a broadening of the energy-loss spectrum, which in our incident energy range can be described by a Gaussian straggling⁴⁶ function

$$f(Q) = \frac{1}{\sqrt{2\pi}\Omega} \exp\left[-\frac{(Q-Q_0)^2}{2\Omega^2}\right],$$

where Ω is the width of the distribution, and Q_0 is the mean value.

IV. DISCUSSION

Let's first have a closer look at the calculations of the particle trajectory lengths (Table III). Figure 11 shows how the trajectory lengths were determined from the MARLOWE data. L is the length the particles stay within a distance d_s near the surface, where d_s is the decay length corresponding to the s electrons as determined in Table I.

For the case of 300 eV and for the [001] directions the numbers given are only rough estimates, since the spread of the trajectories of the outgoing particles is very large, making it difficult to determine the mean trajectory length as described in Fig. 11. For very low energies many particles are scattered off the surface at a distance larger than d_s . Then our approximation, taking advantage of the bulk dielectric function, fails, of course (see Sec. III). For this reason we will not discuss those cases in more detail.

Two important points result from Table III: First, the lengths in symmetrical directions are much larger than in random ones, as expected from Fig. 10. Then, secondly, the trajectory lengths seem to approach a saturation value with increasing energy. For the crystallographic directions it should be noted that the lengths given are an upper limit for the mean trajectory length simply because in those directions the particles penetrate deeper into the surface thereby artificially enlarging the above-defined interaction region.

A. Charge exchange

We start with an analysis of the charge-state experiments, i.e., concentrating on a discussion of the crystallo-

He \rightarrow Ni (110) [Random]
 $\psi = 5^\circ$, $\vartheta = 10^\circ$, $E_0 = 3 \text{ keV}$

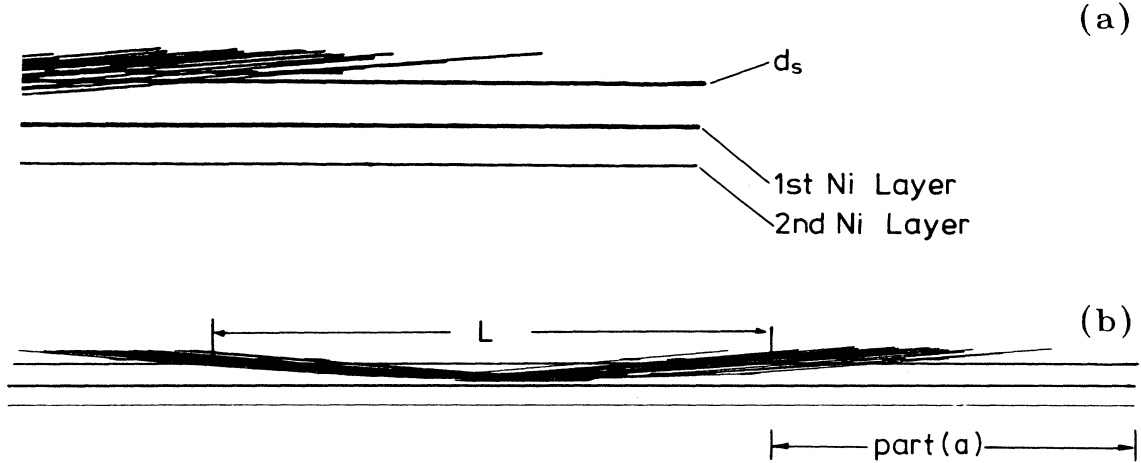


FIG. 11. Sketch of how the trajectory length L was determined from the MARLOWE data. The obtained values are listed in Table III.

graphic dependencies of the charge state fraction based on the experimental numbers summarized in Table II: From Sec. III A we know that the only contributions to charge exchange in our system are Auger capture and dynamic resonant-loss processes. Let $n_t(\text{He}^+)$ be the percentage of He ions at a given time t during the interaction. There are two contributions that change this quantity. On one side there are particles leaving this charge state via Auger neutralization with a probability $1/\tau_A$. (As already stated in Sec. III A we consider only transitions involving s electrons.) On the other side we have particles that are already neutralized at time t , $n_t(\text{He}^0) = 1 - n_t(\text{He}^+)$, but may be reionized via a dynamic resonant-loss process with a probability $1/\tau_R$. We neglect dynamic resonant capture, since its cross section is a factor of about 10 smaller than that for Auger capture.³⁰

This gives the following rate equation for the change of the ion fraction (in the following we omit the index t):

$$\frac{d}{dt}n(\text{He}^+) = -\frac{1}{\tau_A}n(\text{He}^+) + \frac{1}{\tau_R}[1 - n(\text{He}^+)]$$

With $n(\text{He}^+) = 1$ for $t=0$ the solution is

$$n(\text{He}^+) = \frac{\tau}{\tau_R} + \left[1 - \frac{\tau}{\tau_R}\right] e^{-t/\tau}, \quad (1)$$

where

$$\frac{1}{\tau} = \frac{1}{\tau_A} + \frac{1}{\tau_R}$$

The first term of Eq. (1), τ/τ_R , is the equilibrium value of $n(\text{He}^+)$ in the bulk, whereas the second term describes the decay of the initial state. From Ref. 30 we conclude $\sigma_A \gg \sigma_R$, and hence $\tau_R \gg \tau_A$, so that Eq. (1) can be approximated by

$$n(\text{He}^+) = \frac{\tau_A}{\tau_R} + e^{-t/\tau_A}.$$

The time variable t runs from $t=0$, when the particle enters the region where interaction with the surface starts, to $t=T$, when the particle leaves that region. The ion fraction after scattering is then given by

$$n(\text{He}^+) = \frac{\tau_A}{\tau_R} + e^{-T/\tau_A},$$

or by writing things in terms of distance traveled along the surface rather than time,

$$n(\text{He}^+) = \frac{\tau_A}{\tau_R} + e^{-L/\lambda_A}. \quad (2)$$

Here L is the trajectory length the ion is in contact with the surface, and $\lambda_A = v\tau_A$ is a mean free path describing the average length a particle travels near the surface until

TABLE II. Experimental charge-state fraction as defined in Sec. II.

Energy	[$\bar{1}10$]	[001]	Random
3.0 keV	0.016	0.017	0.023
4.9 keV	0.025	0.027	0.035

TABLE III. Trajectory lengths L for different energies determined as indicated in Fig. 11. NC stands for not calculated.

Energy	$[\bar{1}10]$	$[001]$	Random
300 eV	NC	NC	12.0 Å
2.0 keV	47.8 Å	54.9 Å	28.3 Å
3.0 keV	54.5 Å	61.0 Å	32.4 Å
4.9 keV	59.7 Å	64.7 Å	43.0 Å
14 keV	NC	NC	43.0 Å

it is neutralized. It is $\lambda_A = 5.2, 6.3,$ and 8.2 Å for 2-, 3- and 5-keV incident energy, respectively (with $\tau_A = 1.7 \times 10^{-15}$ s). With those values and the trajectory lengths of Table III, the fraction of the initial He^+ still present in the outgoing beam can be evaluated. The numbers are given in Table IV.

We attribute the azimuthal dependence of the ion yield to the *surviving* ions for the following reasons: Once an incoming ion is neutralized, it is reionized with only a very low probability. Those particles which *are* reionized capture an electron again very rapidly via the Auger process and so the reionized particles that finally are detected have lost their electron on the very last part of the exit trajectory where they did not have any further possibility to recapture an electron.

By changing the azimuthal angle the length of the trajectories of the particles is varied. (The angular distribution of the scattered particles is changed, too. We return to this point later.) Any of the trajectory lengths considered for our system (Table III) is much larger than the mean free path λ_A a He ion travels along the surface before it is neutralized. From this we conclude that the yield of the *reionized* particles does not depend on the azimuthal angle. The yield of the surviving ions, on the other hand, *does* depend on the azimuthal angle simply because a longer trajectory “offers more possibilities” to neutralize the ion.

In Eq. (2) the first term on the right-hand side, τ_A / τ_R , gives the azimuth-independent yield of the reionized particles and the exponential describes the azimuthal dependence of the yield of the surviving ions since $L = L(\phi)$. It is instructive to calculate the percentage of surviving ions in the ion peak. For the 3-keV case, for example, one gets for the $[001]$ azimuth 0.3% and for random azimuth 25% surviving ions within the ion peak.

For the channel directions the memory term, $\exp(-L/\lambda_A)$, is very small compared to the random direction. Therefore we use the experimental values of Table II for crystallographic directions to estimate τ_R by neglecting the memory term in those directions:

TABLE IV. Fraction of initial He^+ still present in the outgoing beam for two different energies.

Energy	$[\bar{1}10]$	$[001]$	Random
3.0 keV	1.8×10^{-4}	6.2×10^{-5}	5.8×10^{-3}
4.9 keV	6.9×10^{-4}	3.7×10^{-4}	5.2×10^{-3}

$$\tau_R \simeq \frac{\tau_A}{n_{\text{expt}}(\text{He}^+)}.$$

This yields, for 3 keV, $\tau_R \simeq 1.0 \times 10^{-13}$ s and, for 5 keV, $\tau_R \simeq 6.5 \times 10^{-14}$ s, confirming the inequality $\tau_R \gg \tau_A$.

Now going back to Eq. (1) we can get an estimate of the charge fractions in a *random* direction by inserting the obtained values. This yields, for 3 keV, $n_{\text{random}} \simeq 0.023$ and, for 5 keV, $n_{\text{random}} \simeq 0.031$ consistent with the experimental numbers listed in Table II for random directions.

B. Energy loss

In the following we will use the results obtained concerning the charge state of the particle to explain the energy-loss spectra. The elastic energy loss for a binary collision between He and Ni is calculated from

$$\frac{E}{E_0} = \left[\frac{M_1}{M_1 + M_2} \right]^2 \left\{ \cos\delta + \left[\left(\frac{M_2}{M_1} \right)^2 - \sin^2\delta \right]^{1/2} \right\}^2$$

to be

$$\frac{E}{E_0}(\delta = 10^\circ) = 0.9979,$$

where δ is the scattering angle, and M_1 and M_2 are the masses of the projectile and target atom, respectively. For $E_0 < 5$ keV the elastic energy loss is

$$\Delta Q_{\text{el}} < (1 - 0.9979)E_0 \simeq 10 \text{ eV}$$

for single collisions. For glancing incident angle multiple scattering occurs resulting in $\Delta Q_{\text{el}} \ll 10$ eV. Therefore, we conclude that the energy loss in the system under study is practically due only to inelastic effects. Hence, we define the inelastic loss as the difference Q between the calculated elastic-peak position and the maximum of the energy distribution of the scattered particles.

1. Friction coefficient approach

The energy spectra of reflected neutral He particles for three different incident energies are shown in Fig. 5. We will show that the shape of the curves, which is appreciably more asymmetric than expected in energy-loss experiments, can be accounted for by charge-exchange processes between the incoming ion and the target.

In the following we neglect the dynamic resonant-loss processes, which make only a small contribution to the stopping power. Thus we write the rate equations for the ion and the neutral yield as

$$\frac{dn(\text{He}^+)}{dt} \simeq -\frac{1}{\tau_A} n(\text{He}^+), \quad (3)$$

$$\frac{dn(\text{He}^0)}{dt} \simeq \frac{1}{\tau_A} n(\text{He}^+). \quad (4)$$

Taking into account that the friction coefficient changes with the charge state of the He particle we write for the energy loss before neutralization

$$Q_+(x) = \int_0^x \gamma_s^+ v ds$$

and after neutralization

$$Q_0(x) = \int_x^L \gamma_s^0 v ds$$

so that the total energy loss Q is given by

$$Q = Q_+(x) + Q_0(x) = (\gamma_s^+ - \gamma_s^0)vx + \gamma_s^0 vL, \quad x \in [0, L] \quad (5)$$

where x is the free path for the particle being an ion, and L is the trajectory length. The second term is obtained for $x=0$, i.e., it corresponds to those particles that are neutral along the whole trajectory. Thus the first term gives the additional energy lost by the particle when it is an ion with $(\gamma_s^+ - \gamma_s^0)$ as an effective friction coefficient. We define $Q_0 := Q_0(0)$ and $Q_+ := Q_+(L)$ as the energy loss of a neutral particle and an ion, respectively, which has not changed its charge state during the whole interaction process.

Solving Eq. (3) yields

$$n(\text{He}^+) \simeq \exp\left[-\frac{t}{\tau_A}\right] = \exp\left[-\frac{x}{\lambda_A}\right],$$

and, with this, solving Eq. (4) gives

$$n(\text{He}^0) = 1 - \exp\left[-\frac{x}{\lambda_A}\right]. \quad (6)$$

Transforming variables [see Eq. (5)] by means of

$$x = \frac{Q - Q_0}{(\gamma_s^+ - \gamma_s^0)v}$$

and calculating the derivative with respect to Q yields the energy-loss spectrum for the reflected neutral particles:

$$\frac{dn(\text{He}^0)}{dQ} \propto \exp\left[-\frac{Q - Q_0}{(\gamma_s^+ - \gamma_s^0)v\lambda_A}\right] \times \Theta(Q - Q_0)\Theta(Q_+ - Q), \quad (7)$$

where $\Theta(x)$ is the step function, being 1 (0) for positive (negative) argument. In Fig. 12 we compare the experimental data to the calculated ones. It is important to note that we obtain an asymmetric shape of the distribution by considering the change of the charge state only. But the position of the maximum is shifted with respect to the experiment.

In Eq. (7) the straggling of the energy loss⁴⁶ has been neglected. We include the straggling by convoluting the right-hand side of Eq. (7) with the straggling distribution function, i.e., we calculate

$$\int_0^\infty dQ' \exp\left[-\frac{Q'}{(\gamma_s^+ - \gamma_s^0)v\lambda_A}\right] \times \exp\left[-\frac{(Q' - Q)^2}{2\Omega^2}\right] \Theta(Q' - Q_0)\Theta(Q_+ - Q')$$

which was evaluated using Eq. 3.322 from Ref. 47 to give

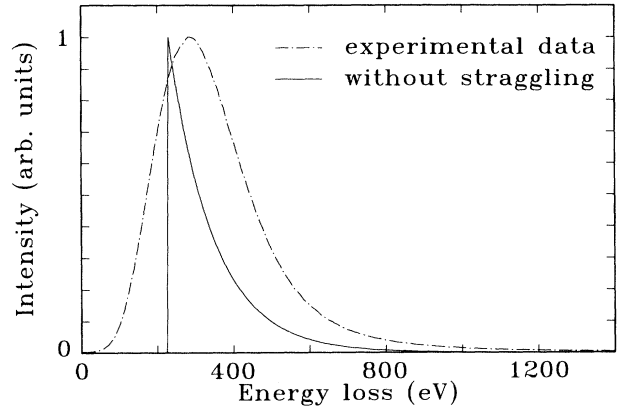


FIG. 12. Comparison of the experimental energy loss with Eq. (7) (without straggling) for the 5-keV case.

$$\frac{dn(\text{He}^0)}{dQ} \propto \exp\left[-\frac{Q - Q_0}{(\gamma_s^+ - \gamma_s^0)v\lambda_A}\right] \times \left[1 + \frac{2}{\sqrt{\pi}} \int_0^y \exp(-t^2) dt\right], \quad (8)$$

where

$$y = \frac{1}{\sqrt{2}} \left[\frac{Q - Q_0}{\Omega} - \frac{\Omega}{(\gamma_s^+ - \gamma_s^0)v\lambda_A} \right].$$

The calculated spectrum depends on the following parameters: τ_A , γ_s^+ , γ_s^0 , and the straggling parameter Ω^2 . The Auger lifetime τ_A has been calculated in Sec. III A; the ratio γ_s^+/γ_s^0 has been calculated in linear theory for an electron gas as a function of the electron density.⁴⁸ The results are given in Table V. We find that a good fit to the experimental data is obtained by taking $\gamma_s^+/\gamma_s^0 = 3.7$, corresponding to an r_s between 1.5 and 2, a density parameter appropriate for Ni. Then γ_s^0 and Ω^2 have been chosen for each energy in such a way that Eq. (8) gives the best fit to our experimental data. The results are shown in Fig. 13. The inclusion of the straggling of the energy loss leads to good agreement between the theoretical and experimental curves. Only when Q_0 and Ω are of similar magnitude—as is the case for 2-keV incident energy—do we find a slight disagreement for energies close to the primary energy.² Table VI shows the values for Q_0 , Ω , and γ_s^0 . We also have calculated Q_0 and Ω using a local-density approach by means of

$$Q_0 = \int_{-\infty}^\infty \gamma_s^0(l)v dl, \quad \Omega^2 = \int_{-\infty}^\infty W(l)dl,$$

TABLE V. Ratio of the friction coefficients for He^+ and He^0 as a function of the “one electron radius” r_s .

r_s (a. u.)	1	2	3	4
γ_s^+/γ_s^0	1.64	4.45	11.95	26.4

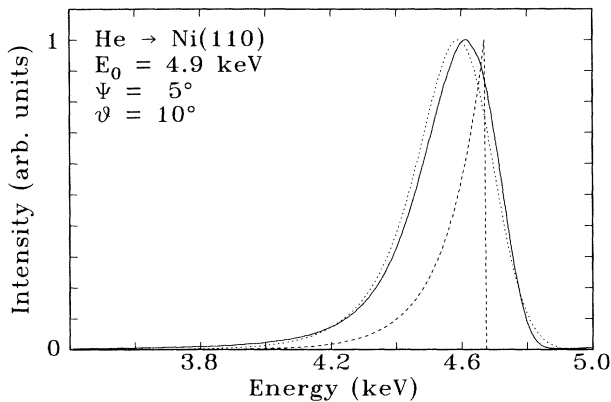


FIG. 13. Energy-loss spectra for emerging He^0 with incident He^+ scattered off Ni(110) for an incident energy of 4.9 keV (angle of incidence 5° , scattering angle 10°). The solid line represents the experimental results, dots are the theoretical result including straggling and the dashed line is the theoretical result excluding straggling.

where γ_s^0 (Fig. 3 in Ref. 49) and W (Fig. 3 in Ref. 50) were obtained locally assuming that they take in each point the values associated with the corresponding electronic local density. Note that these are nonlinear density functional calculations. The results are included in Table VI.

An interesting point is that Eq. (7) can also be obtained by accounting for the exponential decay of the neutralization probability, $1/\tau_A$, and the friction coefficients, γ_s^+ and γ_s^0 , as a function of distance from the surface if we assume that they have the same decay constant.⁵¹

It is important to note that the energy-loss experienced by the ions before entering (and after emerging from) the length L , i.e., the energy loss before (and after) penetrating the interaction region is a small contribution to the total energy loss.⁵² We estimate such a contribution to the loss to be 3 eV for an incident energy of 5 keV.

We mention that another source of straggling is the distribution of trajectory lengths around a mean value \bar{L} . This effect can also be taken into account as a Gaussian broadening of the energy spectra and will be more important for lower velocities, i.e., shorter trajectory lengths; this fact explains why in Table VI the fitted Ω values are larger than the theoretical ones.

It is worth mentioning that $Q_0 = \gamma_s^0 v L$ changes with the particle energy, due not only to v but also to γ_s^0 and L . In the energy range considered here, γ_s^0 (see Table VI) and L (see Table III) are roughly linear in v , suggesting a

TABLE VII. Experimental and calculated values for the energy loss.

Energy	ΔE_{expt}	ΔE_{calc}	$\Delta E_{\text{expt}}/v^3$
2.07 keV	75 eV	80 eV	1004.5 a.u.
3.00 keV	136 eV	150 eV	950.4 a.u.
4.90 keV	287 eV	280 eV	960.8 a.u.

v^3 dependence of Q_0 , a behavior that seems to be followed by the experimental data of Table VII.

2. Convolution method

Up to now we have followed a quite simple approach by describing straggling effects by a Gaussian. Since the particles may even gain energy from the target, one might doubt the correctness of this mean statistical approach. We will demonstrate that the experimental data can also be explained using the so-called “convolution method,”^{53,28} thereby supporting the previous approach. We introduce this method—adapted to our needs—in the following way: First, we assume that the particle loses a fixed amount of energy—say $\hbar\bar{\omega}$ —by creating an excitation in the solid. In the following we will call such an event a “collision.” Referring now to the notations introduced in Fig. 14, we are looking for an expression that gives us the probability $P(n)$ of having n collisions. From this we could calculate the energy spectrum simply by identifying n with the corresponding energy loss $n\hbar\bar{\omega}$.

The probability of suffering n_+ collisions in the interval $[0, x]$, i.e., when it is an ion, is given by

$$\frac{\exp(-x/\lambda_+)}{n_+!} \left[\frac{x}{\lambda_+} \right]^{n_+}.$$

This is the well-known Poisson law, which holds in cases where large numbers of trials (i.e., collisions in our case) are involved with a small probability of occurrence each. With the same argument we get the probability that the then neutral particle suffers n_0 collisions in the interval $[x, L]$:

$$\frac{\exp[-(L-x)/\lambda_0]}{n_0!} \left[\frac{L-x}{\lambda_0} \right]^{n_0}.$$

Taking into account that the probability for the particle being neutralized in the interval $[x, x+dx]$ is given by

$$\frac{dx}{\lambda_A} \exp\left[-\frac{x}{\lambda_A}\right],$$

TABLE VI. Parameters used to fit the energy spectra (marked with a superscript “fit”) and corresponding values from a local-density approximation (LDA).

Energy	Q_0^{fit}	Q_0^{LDA}	Ω^{fit}	Ω^{LDA}	γ_s^0
2.07 keV	49 eV	57.6 eV	38 eV	25.3 eV	0.26 a.u.
3.00 keV	102 eV	96.7 eV	54 eV	39.6 eV	0.37 a.u.
4.90 keV	217 eV	199.4 eV	84 eV	83.6 eV	0.44 a.u.

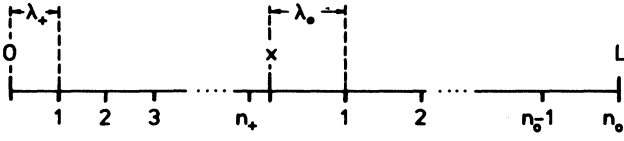


FIG. 14. Schematic sketch of an incoming ion's path near a surface. The interval $[0, L]$ represents that part of the trajectory in which interaction with the surface takes place as defined in Fig. 11. At the point x the ion is neutralized. λ_+ and λ_0 are the mean free paths between collisions for the ion and neutral particle, respectively. Notations above the axis define distances; those below define number of collisions.

where λ_A is the mean free path for the particle being an ion as explained in Sec. III A, we now have an expression that gives us the probability for the particle having n_+ collisions as an ion and n_0 collisions as a neutral particle:

$$P(n_+, n_0) = \int_0^L \frac{dx}{\lambda_A} \exp\left[-\frac{x}{\lambda_A}\right] \frac{\exp(-x/\lambda_+)}{n_+!} \left(\frac{x}{\lambda_+}\right)^{n_+} \times \frac{\exp[-(L-x)/\lambda_0]}{n_0!} \left(\frac{L-x}{\lambda_0}\right)^{n_0}.$$

This can be solved to give

$$P(n_+, n_0) = \frac{(L/\lambda_0)^{n_0} \exp(-L/\lambda_0)}{\lambda_A \lambda_+^{n_+} n_+! \mu^{n_++1}} \times \sum_{k=0}^{n_0} \left(\frac{-1}{L\mu}\right)^k \frac{(n_++k)!}{(n_0-k)!k!} \times \left[1 - e^{-L\mu} \sum_{l=0}^{n_++k} \frac{(L\mu)^l}{l!}\right] \quad (9)$$

where we introduced $\mu = \lambda_A^{-1} + \lambda_+^{-1} - \lambda_0^{-1}$. From Eq. (9) we then calculate the probability that the particle suffers n collisions during its interaction with the surface:

$$P(n) = \sum_{n_+=0}^n P(n_+, n - n_+).$$

We arrived at a discrete energy-loss spectrum $P(\omega)$, where ω only takes the values $\omega = n\bar{\omega}$. In one collision the particle actually does not lose a fixed amount of energy $\hbar\bar{\omega}$ but loses a value $\hbar\omega$, which is distributed around the mean energy loss $\hbar\bar{\omega}$ according to the distribution function $f(\omega)$. Similarly the energy loss for a particle, which has suffered m collisions is distributed around the mean energy loss $m\hbar\bar{\omega}$ with the distribution function $f_m(\omega)$ given by the m -fold convolution of the distribution function for a single collision:

$$f_m(\omega) = \int_0^\omega d\omega' f(\omega') f_{m-1}(\omega - \omega')$$

with $f_0(\omega) = \delta(\omega)$ and $f_1(\omega) = f(\omega)$. In our case, for low-velocity particles, this single spectrum does not present strong asymmetries, since, on one hand, plasmons

cannot be excited and, on the other, tails in the spectrum going as $1/\omega^2$ do not appear (see Chap. 5.2.4 of Ref. 52). Because of this we describe $f(\omega)$ with good accuracy by a Gaussian and accordingly f_m by the m -fold convolution of f :

$$f_m(\omega) = \left[\frac{2}{\pi m \omega_0^2}\right]^{1/2} \exp\left[-\frac{(\omega - m\bar{\omega})^2}{2m\omega_0^2}\right],$$

where ω_0^2 defines the intrinsic straggling of the probability density function $f(\omega)$. With this distribution we obtain the now continuous energy-loss spectrum

$$P(\omega) = \sum_{m=0}^{\infty} P(m) f_m(\omega).$$

In Fig. 15 we show the case of 5 keV, different curves corresponding to the experimental result and to the two different theoretical approaches discussed above.

The relations between stopping power S and mean energy loss per collision $\hbar\bar{\omega}$ on one side and between straggling per unit length W and intrinsic straggling $\hbar\omega_0$ on the other are given by

$$S = \hbar\bar{\omega}/\lambda,$$

$$W = [(\hbar\bar{\omega})^2 + (\hbar\omega_0)^2]/\lambda$$

where λ_+ or λ_0 is to be substituted for λ depending on the charge state of the He particle. The ratio $\lambda_0/\lambda_+ = 3.7$ is the same as for γ_+/γ_0 given above.

In Ref. 54 the differential probability for energy transfer ω in a *single* inelastic excitation process (i.e., creation of an electron-hole pair) was integrated to give the width Γ of the quasiparticle states. From $\Gamma\tau = \Gamma\lambda_0/v \approx 1$ we determined (with $r_s = 1.5$ a.u.) $\lambda_0 = 1.613$ a.u. In Fig. 16 we verified that taking only a single charge state yields Gaussian energy-loss distributions, showing again that the asymmetry in the energy-loss spectra has as origin the change of the charge state during the interaction with the surface.

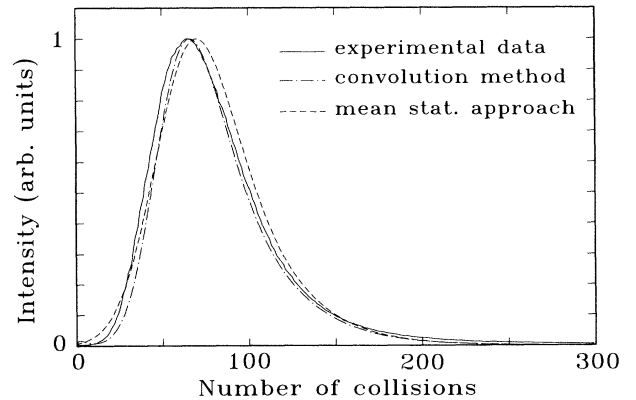


FIG. 15. Energy-loss spectra for a 5-keV incident He^+ on Ni(110) in a random direction.

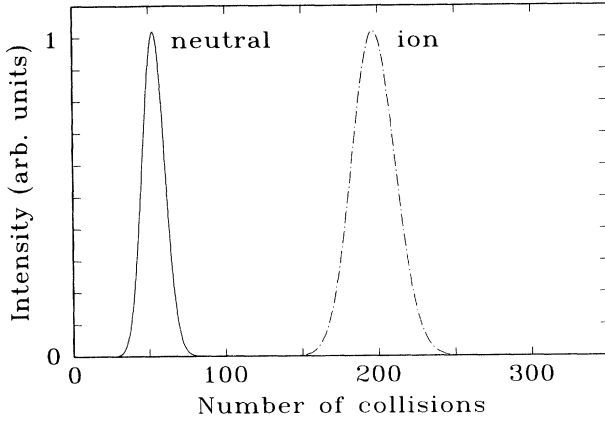


FIG. 16. Energy-loss spectra calculated via the convolution method assuming that the particle is an ion or a neutral particle over the whole trajectory. Incident energy is 5 keV.

3. Symmetric directions and reionization processes

Here we turn our attention to the energy-loss spectra of particles scattered along a crystallographic direction. As mentioned earlier, we will only consider the $[\bar{1}10]$ direction.

Using the same parameters as for random direction, except for the length, which is adjusted according to Table III, yields the curve (d) in Fig. 17. This does not reproduce the experimental curve well. One possible explanation for the high-energy tail is reionization processes. Once a particle is neutralized there is a small probability that it loses its electron in the ground state via dynamic resonant loss thereby losing 24 eV (the ionization energy of He). Since the trajectories are longer in crystallographic directions, we assume that reionization processes are more important there than in random directions.

We start by considering those particles, which have suffered exactly one neutralization and no reionization. The probability of having a neutralization in the interval $[x, x+dx]$ is given by

$$\frac{dx}{\lambda_A} \exp\left[-\frac{x}{\lambda_A}\right],$$

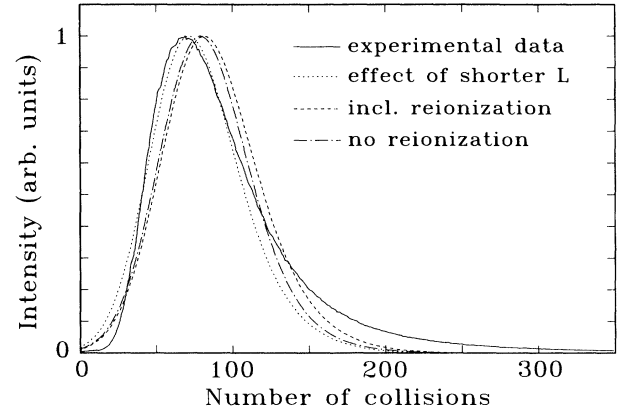


FIG. 17. Energy-loss spectrum for detected He^0 resulting from incoming He^+ scattered off a Ni(110) surface along the $[\bar{1}10]$ direction with an incident energy of 3 keV. Incident angle was 5° , and scattering angle was 10° . The solid line (a) is the experimental data, the dotted line (b) shows how a shorter trajectory length affects the spectrum, the dashed line (c) is the calculated spectrum including reionization, and the dash-dotted line (d) is the calculated spectrum without any reionization considered.

and the probability of not having a reionization in $[x, L]$ is given by

$$1 - \int_x^L \frac{dx'}{\lambda_R} \exp\left[-\frac{(x'-x)}{\lambda_R}\right] = \exp\left[-\frac{(L-x)}{\lambda_R}\right].$$

Hence the probability that an outgoing neutral particle has suffered exactly one neutralization is

$$\begin{aligned} n^{(0)}(\text{He}^0) &= \int_0^L \frac{dx}{\lambda_A} \exp\left[-\frac{x}{\lambda_A}\right] \exp\left[-\frac{(L-x)}{\lambda_R}\right] \\ &= \frac{\lambda_-}{\lambda_A} \left[\exp\left[-\frac{L}{\lambda_R}\right] - \exp\left[-\frac{L}{\lambda_A}\right] \right], \end{aligned}$$

where we introduced $1/\lambda_- = 1/\lambda_A - 1/\lambda_R$. The superscripted (0) indicates “no reionization.”

For $\lambda_R \rightarrow \infty$ the former result, Eq. (6), is recovered. The energy-loss spectrum we now get from

$$\begin{aligned} \frac{dn^{(0)}(\text{He}^0)}{dQ} &= \int_0^L \frac{dx}{\lambda_A} \exp\left[-\frac{x}{\lambda_A}\right] \exp\left[-\frac{(L-x)}{\lambda_R}\right] \delta(Q - Q_0 + (\gamma_s^+ - \gamma_s^0)vx) \\ &= \frac{\exp(-L/\lambda_R)}{(\gamma_s^+ - \gamma_s^0)v\lambda_A} \exp\left[-\frac{Q - Q_0}{(\gamma_s^+ - \gamma_s^0)v\lambda_-}\right] \Theta(Q - Q_0) \Theta(Q_+ - Q). \end{aligned}$$

Analogously we obtain the number of neutral particles arriving at the detector and having suffered exactly one reionization by successively multiplying the probability of having a neutralization in $[x, x+dx]$, a reionization in $[x'-x, x'-x+dx']$, a second neutralization in $[x''-x', x''-x'+dx'']$, and no reionization in $[x'', L]$:

$$n^{(1)}(\text{He}^0) = \exp\left[-\frac{L}{\lambda_R}\right] \int_0^L \frac{dx''}{\lambda_A} \int_0^{x''} \frac{dx'}{\lambda_R} \int_0^{x'} \frac{dx}{\lambda_A} \exp\left[-\frac{x''+x'-x}{\lambda_-}\right].$$

As above we get the energy loss spectrum from

$$\begin{aligned} \frac{dn^{(1)}(\text{He}^0)}{dQ} &= \exp\left[-\frac{L}{\lambda_R}\right] \int_0^L \frac{dx''}{\lambda_A} \int_0^{x''} \frac{dx'}{\lambda_R} \int_0^{x'} \frac{dx}{\lambda_A} \exp\left[-\frac{x''+x'-x}{\lambda_-}\right] \\ &\quad \times \delta(Q - (Q_0 + Q_R) - (\gamma_s^+ - \gamma_s^0)v(x'' - x' + x)) \\ &= \frac{\exp(-L/\lambda_R)}{(\gamma_s^+ - \gamma_s^0)v\lambda_A} \exp\left[-\frac{Q - (Q_0 + Q_R)}{(\gamma_s^+ - \gamma_s^0)v\lambda_-}\right] \frac{Q - (Q_0 + Q_R)}{(\gamma_s^+ - \gamma_s^0)v\lambda_A} \\ &\quad \times \frac{Q_+ + Q_R - Q}{(\gamma_s^+ - \gamma_s^0)v\lambda_R} \Theta(Q - (Q_0 + Q_R)) \Theta(Q_+ + Q_R - Q), \end{aligned}$$

where Q_R is the ionization energy the particle loses during a reionization event. A generalization to the case of k reionizations gives

$$\begin{aligned} \frac{dn^{(k)}(\text{He}^0)}{dQ} &= \frac{\exp(-L/\lambda_R)}{(\gamma_s^+ - \gamma_s^0)v\lambda_A} \exp\left[-\frac{Q - (Q_0 + kQ_R)}{(\gamma_s^+ - \gamma_s^0)v\lambda_-}\right] \left[\frac{1}{k!}\right]^2 \left[\frac{Q - (Q_0 + Q_R)}{(\gamma_s^+ - \gamma_s^0)v\lambda_A}\right]^k \left[\frac{Q_+ + Q_R - Q}{(\gamma_s^+ - \gamma_s^0)v\lambda_R}\right]^k \\ &\quad \times \Theta(Q - (Q_0 + kQ_R)) \Theta(Q_+ + kQ_R - Q). \end{aligned}$$

and the energy-loss spectrum for neutral particles is then obtained by

$$\frac{dn(\text{He}^0)}{dQ} = \sum_{k=0}^{\infty} \frac{dn^{(k)}(\text{He}^0)}{dQ} \quad (10)$$

We calculated the energy-loss spectrum according to Eq. (10) using for the reionization cross section the values calculated in Sec. IV A. This gives curve (c) in Fig. 17. The calculated spectrum is slightly shifted to higher energy losses. As mentioned in the discussion of the MARLOWE calculations, we overestimate the trajectory length in crystallographic directions, which leads to higher energy losses. Therefore we plotted curve (b) in Fig. 17 with a trajectory length reduced by 10% compared to curve (c).

Reionization processes tend to improve the agreement between theory and experiment. Though they cannot account completely for the high-energy-loss tail of the spectrum, the central part could be well fitted by the same parameters used for random directions.

V. CONCLUSION

Experiments on the energy loss and charge exchange for He ions incident on a Ni(110) surface have been performed under grazing incidence (5°) in the incident energy range of 2–5 keV. The azimuthal dependence of the ion as well as of the neutral yield shows evidence for surface channeling when the incident particles are scattered along crystallographic directions. The charge-state fraction exhibits minima in those directions indicating that

Auger neutralization to the ground state is the more effective the longer the trajectory. The Auger lifetime τ_A was calculated from first principles using the dielectric function of bulk nickel. From the experimental data and τ_A we derived an estimate for the dynamic resonant loss lifetime τ_R . Estimates for the trajectory lengths were obtained by calculating the path of the particles in a binary-collision approximation.

The energy-loss spectra of the scattered particles are asymmetric, being skewed to the low-energy side. The spectra for scattering along random directions could be well explained in two ways: first using a friction coefficient approach and introducing a straggling distribution function and second using a convolution method. Including reionization processes gives satisfactory agreement for the energy-loss spectra obtained for scattering along symmetric directions.

ACKNOWLEDGMENTS

Thanks are due to S. Schubert for helpful discussions, and H. Derks for performing the MARLOWE calculations. Financial support by the Deutsche Forschungsgemeinschaft (DFG), the Deutscher Akademischer Austauschdienst (DAAD) as part of the Acciones Integradas Hispano-Alemanas, and the Comisión Asesora de Investigación Científica y Técnica (Contract No. 0388-84) is gratefully acknowledged. One of us (A.N.) gratefully acknowledges the hospitality of the Departamento de la Materia Condensada in Madrid and financial support by the Stifterverband für die Deutsche Wissenschaft.

¹S. K. Allison, Rev. Mod. Phys. **30**, 1137 (1958); **31**, 839(E) (1959).

²A. Närmann, R. Monreal, P. M. Echenique, F. Flores, W. Heiland, and S. Schubert, Phys. Rev. Lett. **64**, 1601 (1990).

³A. Närmann, Mod. Phys. Lett. B **5**, 561 (1991).

⁴B. Willerding, H. Steininger, K. J. Snowdon, and W. Heiland, Nucl. Instrum. Methods Phys. Res. B **2**, 453 (1984).

⁵E. W. Kuipers and A. L. Boers, Nucl. Instrum. Methods Phys. Res. B **29**, 567 (1987).

⁶M. Neumann (private communication).

- ⁷M. Kato, T. Iitaka, and Y. H. Ohtsuki, Nucl. Instrum. Methods Phys. Res. B **33**, 432 (1988).
- ⁸R. Sizmann and C. Varelas, Festkörperprobleme XVII, 261 (1977).
- ⁹M. T. Robinson and I. M. Torrens, Phys. Rev. B **9**, 5008 (1974).
- ¹⁰O. S. Oen and M. T. Robinson, Nucl. Instrum. Methods Phys. Res. **132**, 647 (1976).
- ¹¹D. P. Jackson, Surf. Sci. **43**, 431 (1974).
- ¹²J. F. Ziegler, J. P. Biersack, and U. Littmark, in *Stopping Powers and Ranges of Ions in Matter*, edited by J. F. Ziegler (Pergamon, New York, 1985), p. 1.
- ¹³G. Molière, Z. Naturforsch Teil A **2**, 133 (1947).
- ¹⁴H. Derks, A. Närmann, and W. Heiland, Nucl. Instrum. Methods Phys. Res. B **44**, 125 (1989).
- ¹⁵H. D. Hagstrum, in *Inelastic Ion-Surface Collisions*, edited by N. H. Tolk, J. C. Tully, W. Heiland, and C. W. White (Academic, New York, 1977), p. 1.
- ¹⁶W. Bloss and D. Hone, Surf. Sci. **72**, 277 (1978).
- ¹⁷R. Brako and D. M. Newns, Surf. Sci. **108**, 253 (1981).
- ¹⁸S. I. Easa and A. Modinos, Surf. Sci. **183**, 531 (1987).
- ¹⁹D. M. Newns, K. Makoshi, R. Brako, and J. N. M. van Wunnik, Phys. Scr. T **6**, 5 (1983).
- ²⁰K. J. Snowdon, Nucl. Instrum. Methods Phys. Res. B **33**, 365 (1988).
- ²¹J. C. Tully, Phys. Rev. B **16**, 4324 (1977).
- ²²K. J. Snowdon, R. Hentschke, A. Närmann, and W. Heiland, Surf. Sci. **173**, 581 (1986).
- ²³R. Hentschke, K. J. Snowdon, P. Hertel, and W. Heiland, Surf. Sci. **173**, 565 (1986).
- ²⁴F. Sols, P. Miranzo, and F. Flores, Surf. Sci. **161**, 33 (1985).
- ²⁵F. Sols and F. Flores, Solid State Commun. **42**, 687 (1982).
- ²⁶E. G. d'Agliano, P. Kumar, W. Schaich, and H. Suhl, Phys. Rev. B **11**, 2122 (1975).
- ²⁷R. Núñez, P. M. Echenique, and R. H. Ritchie, J. Phys. C **13**, 4229 (1980).
- ²⁸M. Kato, J. Phys. Soc. Jpn. **55**, 1011 (1986).
- ²⁹N. D. Lang, Solid State Phys. **28**, 225 (1973).
- ³⁰P. M. Echenique, F. Flores, and R. H. Ritchie, Solid State Phys. **43**, 229 (1990).
- ³¹J. H. Weaver, C. Krafka, D. W. Lynch, and E. E. Koch, *Optical Properties of Metals, Physik Daten* (Fachinformationszentrum Energie, Karlsruhe, 1981).
- ³²F. Herman and S. Skillman, *Atomic Structure Calculations* (Prentice-Hall, Englewood Cliffs, 1963).
- ³³D. A. Papaconstantopoulos, *Handbook of the Band Structure of Elemental Solids* (Plenum, New York, 1986).
- ³⁴M. C. Cross, in *Inelastic Ion-Surface Collisions*, edited by N. H. Tolk, J. C. Tully, W. Heiland, and C. W. White (Academic, New York, 1977), p. 253.
- ³⁵F. Sols, Ph.D. thesis, Universidad Autónoma de Madrid, 1985.
- ³⁶W. Heiland and E. Taglauer, Nucl. Instrum. Methods Phys. Res. **132**, 535 (1976).
- ³⁷M. Aono and R. Souda, Nucl. Instrum. Methods Phys. Res. B **27**, 55 (1987).
- ³⁸F. Shoji, K. Oura, and T. Hanawa, Nucl. Instrum. Methods Phys. Res. B **36**, 23 (1989).
- ³⁹U. Fano and W. Lichten, Phys. Rev. Lett. **14**, 627 (1965).
- ⁴⁰D. J. O'Connor and R. J. MacDonald, Nucl. Instrum. Methods Phys. Res. **170**, 495 (1980).
- ⁴¹R. J. MacDonald and D. J. O'Connor, Surf. Sci. **124**, 433 (1983).
- ⁴²W. L. Schaich, Solid State Commun. **15**, 357 (1974).
- ⁴³F. Flores and F. García-Moliner, J. Phys. C **12**, 907 (1979).
- ⁴⁴F. Sols, F. Flores, and N. García, Surf. Sci. **137**, 167 (1984).
- ⁴⁵T. L. Ferrell, P. M. Echenique, and R. H. Ritchie, Solid State Commun. **32**, 419 (1979).
- ⁴⁶M. A. Kumakhov and F. F. Komarov, *Energy Loss and Ion Ranges in Solids* (Gordon and Breach, New York, 1981).
- ⁴⁷I. S. Gradshteyn and I. M. Ryzhik, *Table of Integrals, Series and Products* (Academic, New York, 1980) (corrected and enlarged edition).
- ⁴⁸T. L. Ferrell and R. H. Ritchie, Phys. Rev. B **16**, 115 (1977).
- ⁴⁹P. M. Echenique, R. M. Nieminen, J. C. Ashley, and R. H. Ritchie, Phys. Rev. A **33**, 897 (1986).
- ⁵⁰J. C. Ashley, A. Gras-Martí, and P. M. Echenique, Phys. Rev. A **34**, 2495 (1986).
- ⁵¹K. Schmidt, Master's thesis, Universität Osnabrück, 1989.
- ⁵²F. García-Moliner and F. Flores, *Introduction to the Theory of Solid Surfaces* (Cambridge University Press, Cambridge, 1979).
- ⁵³H. Bichsel, Rev. Mod. Phys. **60**, 663 (1988).
- ⁵⁴I. Nagy, A. Arnau, and P. M. Echenique, Phys. Rev. B **38**, 9191 (1988).